Rare Metal Materials and Engineering
Volume 49, Issue 11, November 2020
Available online at www.rmme.ac.cn

Science Press

Cite this article as: Rare Metal Materials and Engineering, 2020, 49(11): 3653-3661.

ARTICLE

Hot Deformation Behavior and Mechanism of As-cast Ti-5553 Alloy with Coarse Grains

Zhao Qinyang[1], Chen Yongnan[1], Xu Yiku[1], Leandro Bolzoni[2], Fei Yang[2]

[1] Chang'an University, Xi'an 710064, China; [2] University of Waikato, Hamilton 3240, New Zealand

Abstract: The hot deformation behavior of as-cast Ti-5553 (Ti-5Al-5Mo-5V-3Cr) alloy with coarse grain was investigated in the temperature range of 700~1100 °C and strain rate range of 0.001~10 s^{-1} by Gleeble-3800 thermal physical simulator. The results show that the flow stress is sensitive to both temperature and strain rate, and the flow curves display various softening modes under different conditions. The activation energy map and constitutive relationship are constructed for the alloy, and the average deformation activation energy is calculated as 447.2 kJ/mol. The hot processing map is established based on the dynamic materials model with the identification of underlying mechanisms at various processing regions. Two peak domains are identified in the hot processing map: 800~975 °C/0.001~0.01 s^{-1} and 1000~1100 °C/0.01~0.1 s^{-1}, and the flow instability region locates at the region where the strain rate is higher than 1 s^{-1}. External cracking, adiabatic shear banding and/or flow localization are observed in the region of low-temperature deformation and flow instability, and these conditions should be avoided in actual processing. The mechanism at the peak efficiency domain is dynamic recovery (DRV) or the combination of DRV and dynamic recrystallization (DRX), and the region with the occurrence of extensive DRX is recommended as the optimal processing window for the alloy at high temperature about 1100 °C and medium-low strain rate about 0.01 s^{-1}.

Key words: Ti-5553 alloy; hot deformation; constitutive relationship; processing map; deformation mechanism

Titanium and its alloys have drawn great attention and become the research hotspot in high-performance engineering and biomedical fields, thanks to their excellent balanced properties, such as very high strength-density ratio, outstanding corrosion resistance, wide service temperature range and excellent biocompatibility [1]. Particularly, the branch of metastable β titanium alloy has been newly developed for commercial aerospace and marine applications, because of their extra merits of ultra-high-strength with reasonable toughness and good hardenability [2-4]. This makes the metastable β titanium alloys have great potential in replacing those heavier high-strength and stainless steels used in the related fields. Ti-5553 (Ti-5Al-5Mo-5V-3Cr) alloy is a kind of metastable β titanium alloy, which has been successfully used for aerospace industry as landing gear and framework in military and civil aircrafts [5].

Moreover, the aforementioned outstanding mechanical performance of metastable β titanium alloys is highly dependent on the thermo-mechanical processing (TMP, like forging, extrusion and rolling) which shapes the appearance effectively and varies the microstructure irreversibly of the alloys. Nevertheless, metastable β titanium alloys are extremely sensitive to the processing parameters due to their complicated/active phase transformation and strong microstructure heredity compared to other titanium alloys. In addition, the microstructure variation of titanium alloys during TMP is associated with the softening mechanism greatly. Therefore, it is essential to study the hot deformation behavior, determine the optimized hot processing window and identify the underlying mechanism for metastable β titanium alloys to achieve precise microstructure control and realize ideal property optimization during TMP.

Due to the high significance of TMP and underlying mechanism for metastable β titanium alloys, a large number

Received date: February 29, 2020
Foundation item: New Zealand Ministry of Business, Innovation and Employment (UOWX1402)
Corresponding author: Zhao Qinyang, Ph. D., School of Materials Science and Engineering, Chang'an University, Xi'an 710064, P. R. China, Tel: 0086-29-82337340, E-mail: zqy_ustb@163.com

of research has been carried out to investigate the hot deformation behavior and related microstructural evolution of the alloys, including Ti-5553 alloy. Bao et al [6] built the hot processing map and revealed the effect of initial microstructure on the flow behavior of Ti-1023 (Ti-10V-2Fe-3Al) alloy. Hua et al [7] investigated the hot deformation behavior and microstructure evolution situation of forged Ti-5553 alloy bar. Fan et al [8] demonstrated the optimal processing window with excellent hot workability and revealed the dominant mechanism at various processing regions of the newly-developed Ti-7333 (Ti-7Mo-3Nb-3Cr-3Al) alloy in as-processed condition. Matsumoto et al [9] investigated the microstructure evolution characteristics of processed single-β-phase Ti-5553 alloy. Zhou et al [10,11] studied the dynamic recrystallization (DRX) behavior of the forged Ti-5553 alloy bar and determined the critical conditions for the occurrence of DRX in the alloy.

It can be found that the previous research on the hot deformation behavior for metastable β titanium alloy is mainly conducted on the alloys in as-processed condition. However, TMP of titanium alloys should be firstly performed on the as-cast material for ideal shaping and microstructure/property optimization. More importantly, the hot deformation response of as-cast Ti-5553 alloy nearly remains blank, and needs to be well addressed. Additionally, the alloy in as-cast state usually has large grains in the microstructure, which is much coarser than the alloy after multiple-pass processing with refined microstructure. Consequently, it is necessary to study the hot deformation behavior of as-cast alloy instead of the already processed alloy to provide theoretical support and technical guidance for the actual TMP of metastable β titanium alloys.

Currently, Ti-5553 metastable β titanium alloy in as-cast state was employed in the research to investigate its hot deformation behavior including flow behavior and microstructure evolution characteristics, accompanied by the establishment of constitutive relationship and processing map. Particularly, the detailed deformation mechanism was revealed and linked to the constructed maps to provide a comprehensive evaluation for the hot workability of alloy in different processing regions.

1 Experiment

The Ti-5553 alloy (Ti-5.14Al-5.02Mo-5.03V-3.10Cr-0.08O) investigated in this research was obtained from a 35 kg alloy ingot with cylindrical shape prepared by conventional double vacuum arc remelting (VAR) and casting, whose initial microstructure is shown in Fig.1. Obviously, the alloy in as-cast state possesses a very coarse microstructure with large prior β grain and fine α precipitates, and the β grain size is higher than 1000 μm. Moreover, the β phase transformation temperature of the alloy is determined as 875±5 °C by heat treatment and metallographical examination.

Hot deformation testing was performed on a Gleeble® 3800-GTC thermal physical simulator in the mode of isothermal compression using cylinder specimens with 10 mm in diameter and 15 mm in height. The specimens were obtained from the alloy ingot by electrical discharge machining and subsequent precise machining to the target dimension. The compression parameter was set at the temperature of 700 °C to 1100 °C (100 °C interval) and the strain rates of 0.001, 0.01, 0.1, 1 and 10 s^{-1}, until total deformation degree of 70% specimens' height reduction in vacuum. The specimen was heated up to the testing temperature at a constant heating rate of 10 °C/s, and then kept for 4 min to ensure the thermal equilibrium throughout the specimen. Pt-Rh thermal couple was welded on the center surface of the specimen to measure the temperature during the whole compression process dynamically. Tantalum sheets and graphite foils were placed between the anvil and specimen to reduce the friction and improve the electroconductivity of the testing system. Upon the completion of compression testing, all the compressed specimens were quenched immediately in water to retain the deformed microstructure for further examination. During hot compression, the stress-strain relationship and the actual temperature of the specimens were recorded by the system automatically.

The compressed specimens were sectioned equally along the longitudinal direction for microstructural observation. The metallographic specimens were prepared by standard grinding, polishing and etching (modified Kroll's reagent: 10 vol% HF, 20 vol% HNO_3 and 70 vol% H_2O) processes and then examined by optical microscopy (OM, OLYMPUS-PMG3) and scanning electron microscopy (SEM, JSM-6460). For transmission electron microscopy (TEM) observation, the round specimen with a size of 3 mm was ground to 60 μm and then punched from the compressed specimen. After twin-jet electro-polishing, the thin slice was examined by JEM-2100 facility.

2 Results and Discussion

2.1 Flow behavior

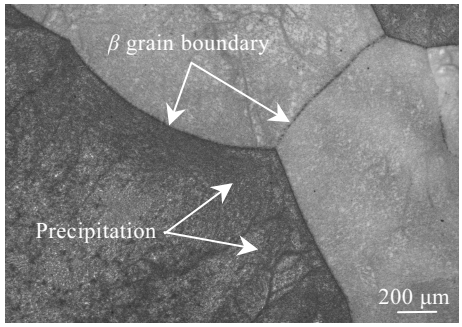

Fig.1 Initial microstructure of as-cast Ti-5553 alloy

Fig.2 shows the true stress-true strain curves of the alloy deformed at various temperatures and strain rates. Generally speaking, the flow stress of the alloy increases rapidly at the beginning of the deformation until the peak flow stress and then drops down gradually (such as Fig.2b) to a steady level (referred to as steady-state stress) or keeps at almost the peak stress until the end of deformation (such as Fig.2c). Obviously, as shown in Fig.3, both the peak flow stress and steady-state stress of the alloy increase with enhancing the strain rate but increase with reducing the deformation temperature. Moreover, the temperature sensitivity of the stress is higher when the alloy is deformed at (α+β) region than at β region. The negative sensitivity of the flow stress to the temperature is that the elemental diffusion and thermal activation will be further promoted at high temperatures. Meanwhile, the increased velocity of mobile dislocation in high-strain-rate deformation causes a positive correlation between flow stress and strain rate [8].

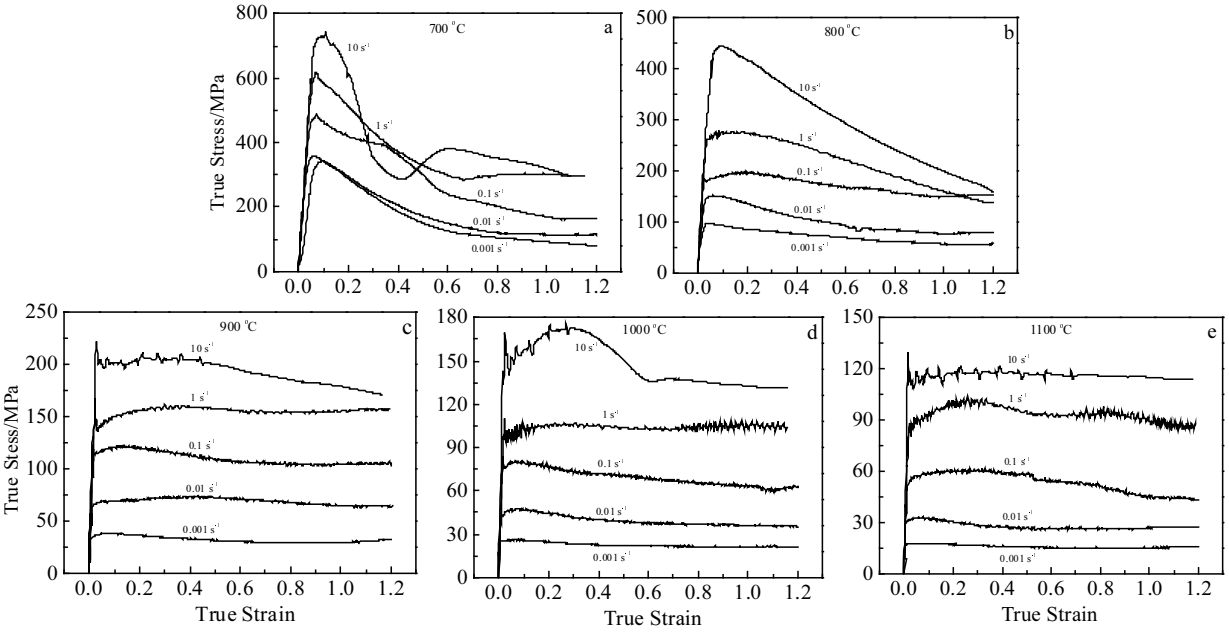

Fig.2 True stress-true strain curves of as-cast Ti-5553 alloy deformed under various conditions: (a) 700 °C, (b) 800 °C, (c) 900 °C, (d) 1000 °C, and (e) 1100 °C

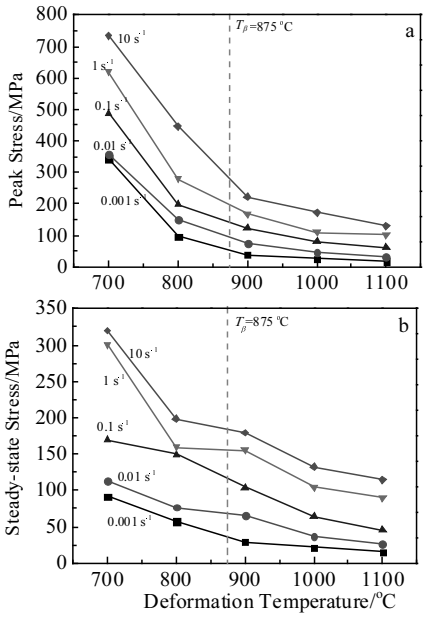

Fig.3 Variation of peak flow stress (a) and steady-state stress (b) with deformation temperature and strain rate

Actually, the hot deformation of metallic materials is achieved by the dynamic competition of work hardening and flow softening. Work hardening plays the dominant role at early deformation, leading to the sharp increment of the flow stress, while the effect of flow softening becomes stronger and stronger gradually. In most conditions, the balance between work hardening and flow softening is reached at later deformation, reflecting as the steady-state of the flow stress. Different flow softening modes of the curves indicate that the active deformation mechanism can be varied. The appearance of steady-state of the flow stress indicates that the active mechanism may be dynamic recovery (DRV), DRX and/or evolution of α phase [12]. Conversely, when the flow stress decreases continuously after the peak point till the end of the deformation, it is demonstrated that the effective mechanism is likely to be flow instability such as external damage, flow localization (FL) and shear banding [13]. As analyzed above, it is difficult and confused to determine the deformation mechanism of the alloy under various conditions only by interpreting the shape of the flow curves, because different microstructural

variation modes may cause similar phenomenon when it comes to flow behavior. Therefore, kinetic analysis and microstructural observation are needed to understand the underlying mechanism of the alloy when it is processed under various conditions.

2.2 Constitutive relationship

Zener-Hollomon parameter (Z) is widely applied to describe the internal relationships between flow stress, strain rate and temperature for the metallic materials during hot deformation, as the well-known constitutive equation:

$$Z=\dot{\varepsilon}\exp(Q/RT)=f(\sigma) \quad (1)$$

where $\dot{\varepsilon}$ is strain rate, Q is the apparent deformation activation energy, R is the universal gas constant, σ is flow stress and T is the absolute temperature. After that, Arrhenius-type constitutive equation given by Sellars and McTegart [14] is widely-accepted to resolve the function of $f(\sigma)$ in Eq.(1), in which the most applicable one in the wide range of deformation temperatures and strain rates is employed here to convert Eq.(1) as follows:

$$Z=\dot{\varepsilon}\exp(Q/RT)=A[\sinh(\alpha\sigma)]^n \quad (2)$$

where A and α are constants, and n is stress exponent ($n = 1/m$, m is strain rate sensitivity), which is defined by

$$n=\{\frac{\partial \ln \dot{\varepsilon}}{\partial \ln[\sinh(\alpha\sigma)]}\}_T \quad (3)$$

Hereinafter, the activation energy (Q) can be defined as follows:

$$Q=R\{\frac{\partial \ln \dot{\varepsilon}}{\partial \ln[\sinh(\alpha\sigma)]}\}_T\{\frac{\partial \ln[\sinh(\alpha\sigma)]}{\partial(1/T)}\}_{\dot{\varepsilon}} \quad (4)$$

Moreover, the constant α can be obtained by the following equations:

$$\alpha=\beta/n_1 \quad (5)$$

$$n_1=(\frac{\partial \ln \dot{\varepsilon}}{\partial \ln \sigma})_T \quad (6)$$

$$\beta=(\frac{\partial \ln \dot{\varepsilon}}{\partial \sigma})_T \quad (7)$$

Based on the above equations, in order to calculate the constants and Q for the equations at peak flow stress, the linear fitting plots of σ-$\ln\dot{\varepsilon}$, $\ln\sigma$-$\ln\dot{\varepsilon}$, $\ln[\sinh(\alpha\sigma)]$-$\ln\dot{\varepsilon}$ and $\ln[\sinh(\alpha\sigma)]$-$1/T$ are given in Fig.4 and Fig.5. In particular, the average value of α at various temperatures is adopted for further calculation. Then the distribution of Q (at peak stress) with varying the temperature and strain rate can be obtained and is shown in Fig.6 as a three-dimensional map. As shown in Fig.6, the value of Q is sensitive to both strain rate and temperature. The value of Q increases with increasing both the strain rate and temperature and is in the

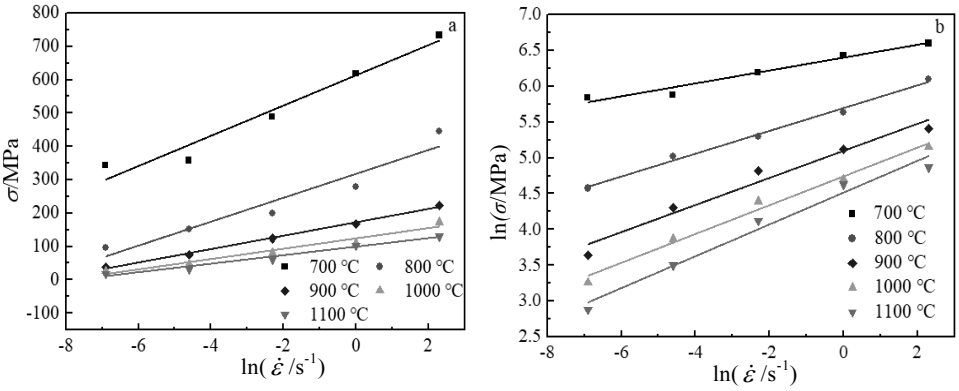

Fig.4 Linear fitting of peak flow stress and strain rate: (a) σ-$\ln\dot{\varepsilon}$ and (b) $\ln\sigma$-$\ln\dot{\varepsilon}$

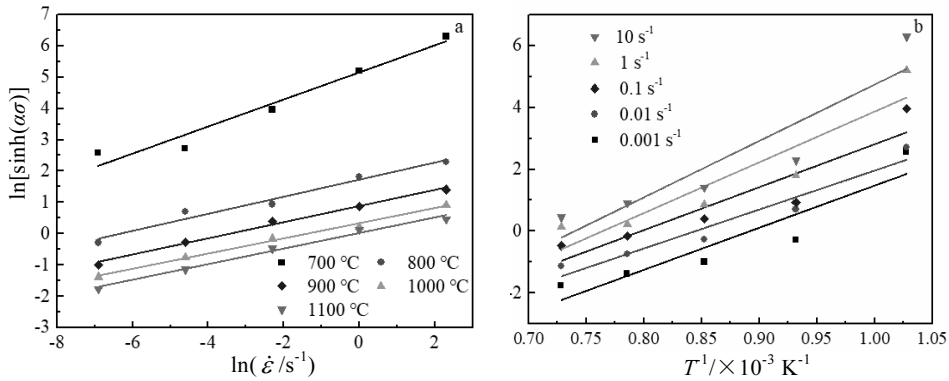

Fig.5 Arrhenius-type plot showing the variation of flow stress with temperature and strain rate: (a) $\ln[\sinh(\alpha\sigma)]$-$\ln\dot{\varepsilon}$ and (b) $\ln[\sinh(\alpha\sigma)]$-T^{-1}

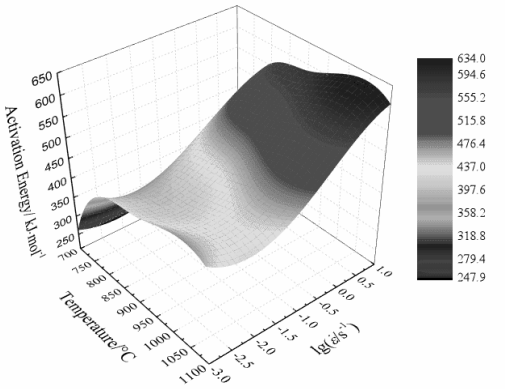

Fig.6 Three-dimensional deformation activation energy (at peak flow stress) distribution map of as-cast Ti-5553 alloy with changing temperature and strain rate

range of 242.3~625.2 kJ/mol, and the average Q under all processing conditions is calculated as 447.2 kJ/mol. This average value is higher than that of other as-processed metastable β titanium alloys like Ti-7333, Ti-5553 and Ti-1300 [8,15,16]. This result may be caused by the much larger grain size of the as-cast alloy, which consumes more external energy to reform the grain structure. Moreover, it has been confirmed that the region with nearly constant Q in the activation energy map can be considered as a potential optimal processing window for metallic materials with good hot workability [17]. There is a nearly-flat surface of Q at the region of 975~1100 °C/0.001~0.1 s^{-1} for the alloy with Q between 430 and 450 kJ/mol, demonstrating that the optimal processing window may suit within this region. In contrast, other regions show the relatively high/low value with significant fluctuation, which indicates the possibility for the occurrence of flow instability.

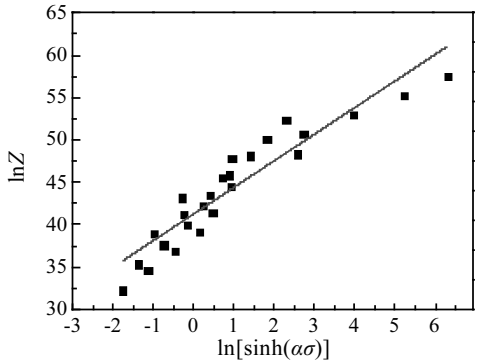

Fig.7 Relationship between peak flow stress and the Zener-Hollomon parameter

After performing natural logarithm, Eq.(2) can be rearranged into the following format:

$$\ln Z=\ln A+n\ln[\sinh(\alpha\sigma)] \tag{8}$$

The linear fitting of ln$Z$ and ln[sinh ($\alpha\sigma$)] is shown in Fig.7 for the final constitutive equations. The values of ln$A$ and n can be obtained by the intercept and slope of the fitting line as 41.25 and 3.14, respectively. Then, substituting the values of deformation activation energy Q (average), stress exponent n, constants ln$A$ and α into Eq.(2), one of the constitutive equations of the as-cast Ti-5553 alloy when it is subjected to strain rate, is obtained as follows:

$$\dot{\varepsilon}=\mathrm{e}^{41.25}[\sinh(0.009\ 53\sigma)]^{3.14}\exp[-447\ 200/RT] \tag{9}$$

Furthermore, based on the hyperbolic sine function, Eq.(2) can be rearranged into another type of hot deformation constitutive equation:

$$\sigma=\frac{1}{\alpha}\ln\{(\frac{z}{A})^{1/n}+[(\frac{z}{A})^{2/n}+1]^{1/2}\} \tag{10}$$

Then, the relationship between flow stress and Zener-Hollomon parameter of the alloy can be obtained by substituting the values of the calculated constants:

$$\sigma=\frac{1}{0.0953}\ln\{(\frac{z}{8.22\times10^{17}})^{\frac{1}{3.14}}+[(\frac{z}{8.22\times10^{17}})^{\frac{2}{3.14}}+1]^{\frac{1}{2}}\} \tag{11}$$

The constructed equations can be employed to evaluate the hot deformation resistance of alloy during the actual TMP under different conditions and provide a theoretical basis for the choice of industrial processing facilities with suitable tonnage and parameters.

2.3 Hot processing map

Hot processing map is an effective and widely-used approach to investigate the hot deformation behavior, microstructural evolution and corresponding deformation mechanism of metallic materials, which is developed based on the dynamic materials model (DMM) introduced by Prasad et al[18] and mainly modified by Murty et al [19]. In this mode, the material under TMP is regarded as a power dissipater in the closed adiabatic system. The power dissipation efficiency (η) represents the energy absorption proportion for microstructural changes against the heat conversion of the material during processing and is related to co-content J and strain rate sensitivity m:

$$\eta=\frac{J}{J_{\max}} \tag{12}$$

where

$$J=\int_0^{\dot{\varepsilon}}\sigma\,\mathrm{d}\,\dot{\varepsilon} \tag{13}$$

$$\sigma=C\dot{\varepsilon}^{m} \tag{14}$$

$$m=(\frac{\dot{\varepsilon}\partial\sigma}{\sigma\partial\dot{\varepsilon}})_{T,\varepsilon}=(\frac{\partial\ln\sigma}{\partial\ln\dot{\varepsilon}})_{T,\varepsilon} \tag{15}$$

$$J_{\max}=\frac{\sigma\dot{\varepsilon}}{2} \tag{16}$$

Then the calculation of η can be achieved by:

$$\eta = \frac{2m}{m+1} \tag{17}$$

Next, the continuum criterion of flow instability is provided, which is given based on the extremum principles of irreversible thermodynamics:

$$\xi(\dot{\varepsilon}) = \frac{\partial \ln(\frac{m}{m+1})}{\partial \ln \dot{\varepsilon}} + m < 0 \tag{18}$$

The variations of η and ξ with deformation temperature and strain rate construct the power dissipation map and flow instability map, respectively. Fig.8a and 8b display the 3D power dissipation map and 2D flow instability map of the alloy at the true strain of 0.6, respectively.

The region with a relatively high value of η suggests significant dynamic microstructural changes, like DRX, DRV, phase morphology evolution and superplastic deformation, by which the excellent hot workability of the alloy may be achieved. For the flow instability map, unstable deformation is expected to occur in the region with negative ξ value. Superimposing the instability map over the power dissipation map, the establishment of an integrated hot processing map is achieved, as shown in Fig.9. It is verified for titanium alloys that the processing region with η higher than 35% can be considered as the optimal processing window, which is commonly decided by the alloy's high stacking energy [20]. As shown in Fig.9, there are mainly two domains with high η, which are located under the conditions of 800~975 °C/0.001~0.01 s^{-1} (domain A) and 1000~1100 °C/0.01~0.1 s^{-1} (domain B), with the peak η value of 65% and 46%, respectively. Meanwhile, it is also illustrated in Fig.9 that there is a consecutive and wide flow instability domain which locates at the region with strain rate higher than 1 s^{-1}, no matter what the deformation temperature is.

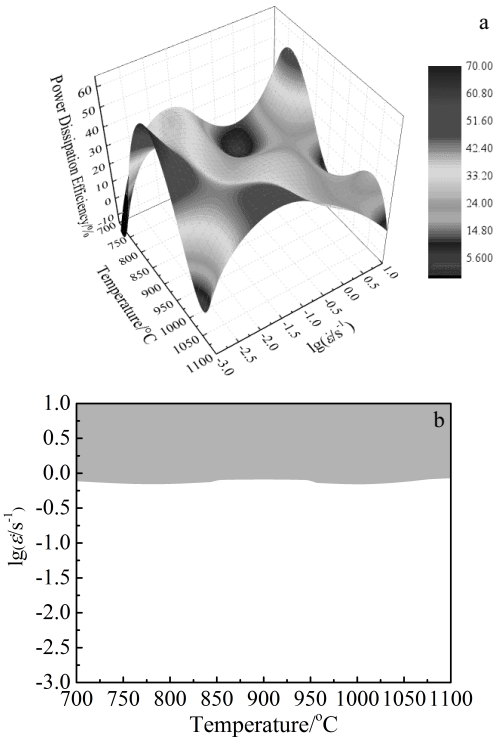

Fig.8 Individual maps for the construction of hot processing map at the strain of 0.6: (a) 3D power dissipation map and (b) 2D flow instability map

Although the flow behavior and thermodynamic/kinetic analysis have been investigated and conducted to evaluate the hot workability of the alloy, microstructural evolution characteristics of the alloy under typical conditions are still needed to be uncovered for verifying the reliability of the optimum processing parameters predicted by the hot processing map and revealing the underlying deformation mechanism.

2.4 Microstructural evolution

Fig.10 shows the macroscopic appearance of the alloy deformed at 700 °C, and it is clear that external cracking is found outside all the specimens, indicating the occurrence of serious flow instability under these conditions. The degree of external cracking is higher at large deformation strain rate, as revealed in Fig.10b and 10c. Particularly, 45° fracture is found for the specimen deformed at 700 °C/10 s^{-1}, and the corresponding flow curve (Fig.2a) shows a significant stress drop at the strain between 0.2 and 0.6, demonstrating a good unity of the flow behavior and fracture mode of the alloy. Besides the external cracking, as shown in Fig.11, adiabatic shearing banding (ASB) is also observed in the microstructure of the alloy deformed at 700 °C. Therefore, it can be concluded that the deformation mechanism is external cracking and ASB at 700 °C, and processing of the alloy is unstable at such a low temperature.

Fig.12 shows the microstructure of the alloy deformed at 800 and 900 °C. As shown in Fig.12a~12c, FL is observed when the deformation condition is 800 °C/1 s^{-1}, and the microstructure is covered by massive α precipitates at 0.1 and 0.001 s^{-1}. Moreover, the TEM images shown in Fig.13a and

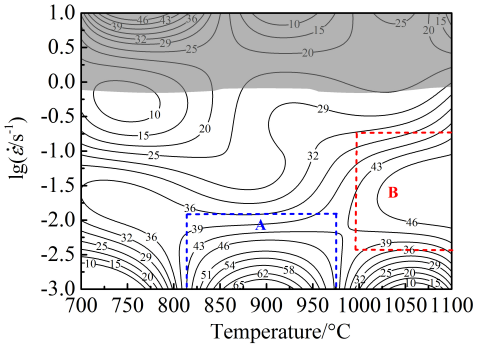

Fig.9 Hot processing map of as-cast Ti-5553 alloy at the strain of 0.6 (contour numbers represent the power dissipation efficiency η, and the grey-shaded regions represent the instability domains)

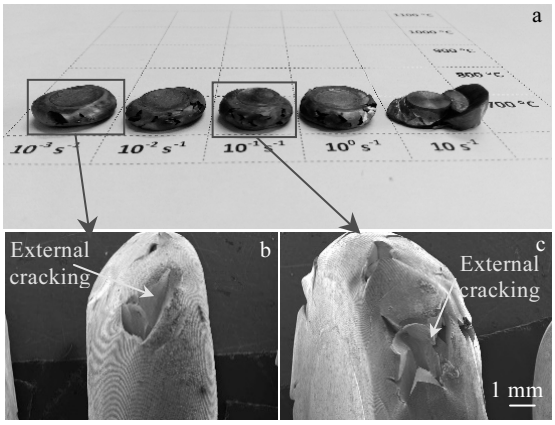

Fig.10 Macroscopic morphologies (a) and SEM images of the alloy deformed at 700 °C/0.001 s^{-1} (b) and 700 °C/0.1 s^{-1} (c)

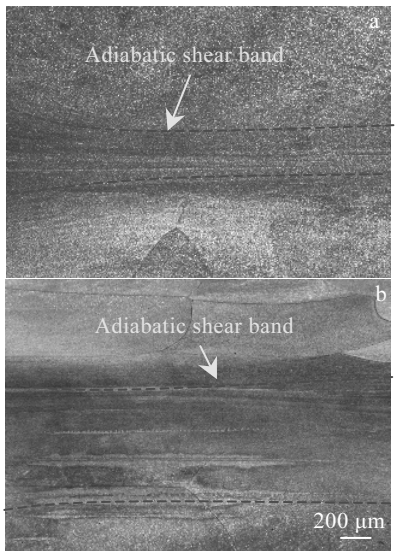

Fig.11 OM microstructures of the alloy deformed at 700 °C and various strain rates: (a) 0.001 s^{-1} and (b) 0.1 s^{-1}

13b reveal that α precipitates deformed at 800 °C are in the shape of large plate, and dislocation accumulation is found around and inside the α plate. In Fig.13a, the fracturing of α plate is also captured, as a result of local stress concentration. From the above results, the dominated deformation mechanism of the alloy deformed at 800 °C is FL (high strain rate) and dynamic α precipitation/fracturing (low strain rate).

As shown in Fig.12d, FL is also observed under the deformation condition of 900 °C/10 s^{-1}. With decreasing the strain rate to 0.1 s^{-1} at 900 °C, serrated grain boundaries with coarse grains are found in Fig.12e, indicating that β-DRV becomes the active deformation mechanism. With further lowering the strain rate to 0.001 s^{-1} (Fig.12f), small equiaxial grains are witnessed in the microstructure together with serrated β grain boundaries, which mean that the dominated mechanism is the combination of β-DRV and β-DRX. The presence of strong DRV effects at 900 °C (0.1 s^{-1} and 0.001 s^{-1}) is also confirmed by the TEM images in Fig.13c and 13d with the emergence of sub-grain boundary formed based on tangled dislocations and dislocation wall.

Fig.14 shows the microstructure of the alloy deformed at 1000 and 1100 °C. A small proportion of DRX grains are observed when the alloy is deformed at 10 s^{-1} at these two temperatures (Fig.14a and 14d), whereas the appearance of the corresponding specimens suggests local kinking features. Therefore, the active deformation mechanism can be speculated as flow instability and β-DRX. With reducing the strain rate to 1 and 0.01 s^{-1} (Fig.14b and 14c), both DRV and DRX characteristics can be found in the microstructure of the alloy deformed at 1000 °C. Besides β-DRV, significant β-DRX and extensive β-DRX are revealed when the alloy is deformed under 1100 °C/0.1 s^{-1} (Fig.14e) and 1100 °C/0.01 s^{-1} (Fig.14f), respectively, characterized by a large number of small equiaxial grains within the prior β grain.

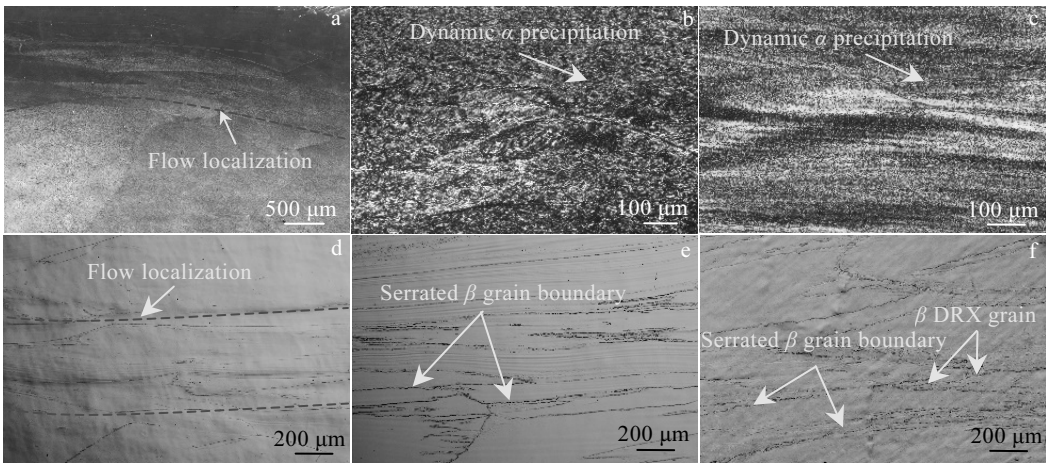

Fig.12 OM microstructures of the alloy deformed at medium temperatures and various strain rates: (a) 800 °C/1 s^{-1}, (b) 800 °C/0.1 s^{-1}, (c) 800 °C/0.001 s^{-1}, (d) 900 °C/10 s^{-1}, (e) 900 °C/0.1 s^{-1}, and (f) 900 °C/0.001 s^{-1}

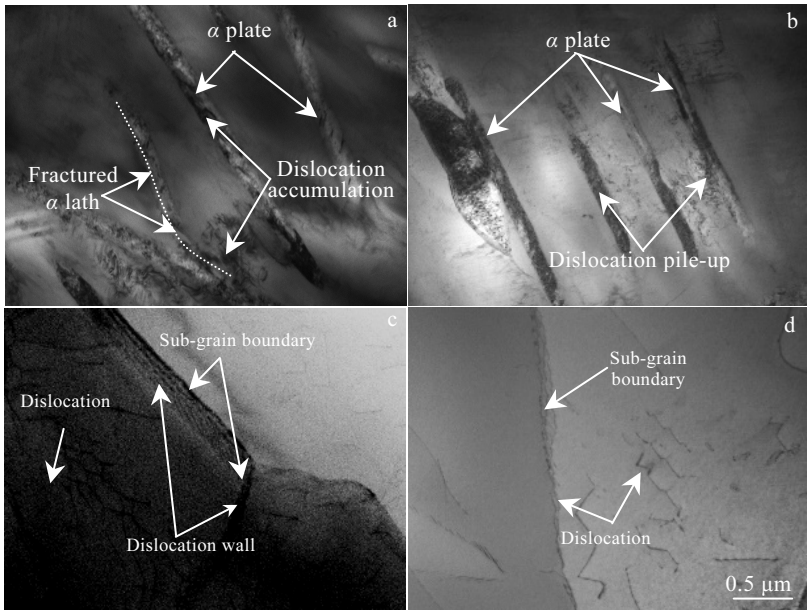

Fig.13 TEM microstructures of the alloy deformed at medium temperatures and various strain rates: (a) 800 °C/1 s^{-1}, (b) 800 °C/0.001 s^{-1}, (c) 900 °C/0.1 s^{-1}, and (d) 900 °C/0.001 s^{-1}

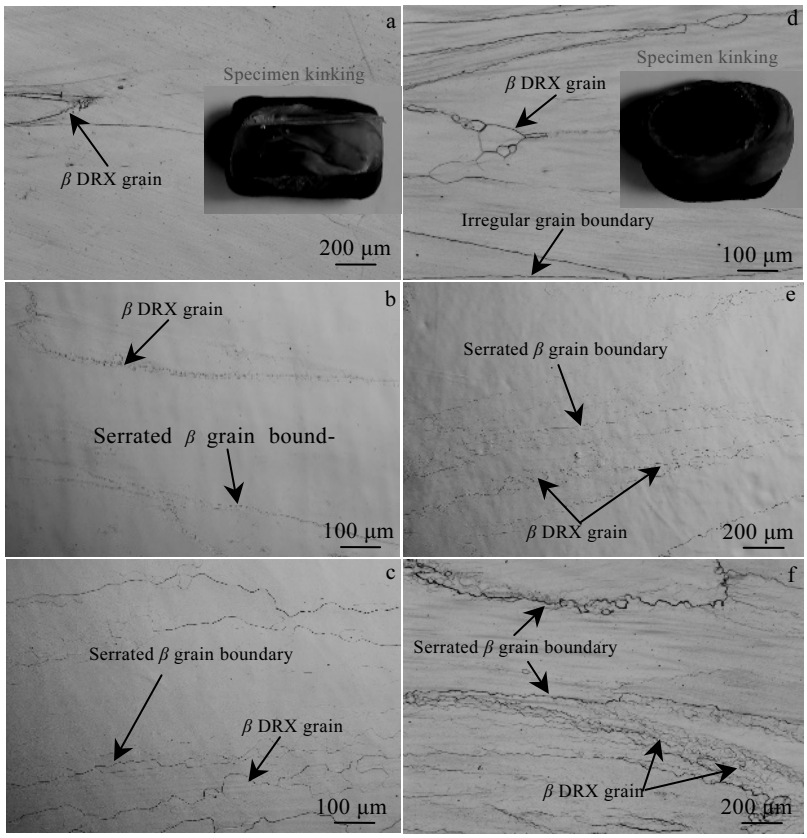

Fig.14 OM microstructures and macroscopic morphologies of the alloy deformed at high temperatures and various strain rates: (a) 1000 °C/10 s^{-1}; (b) 1000 °C/1 s^{-1}; (c) 1000 °C/0.01 s^{-1}; (d) 1100 °C/10 s^{-1}; (e) 1100 °C/0.1 s^{-1}; (f) 1100 °C/0.01 s^{-1}

From above microstructural observation, it is clear that the activation energy map, processing map and microstructural evolution results show a high consistency with the hot deformation behavior of the alloy. The processing conditions within the flow instability region of the processing map are verified to cause external cracking, ASB, FL and local kinking for the alloy, which should be avoided in actual TMP. Moreover, the optimal processing regions (do-

mains A and B in Fig.9) predicted by the processing map is governed by DRV+DRX and DRX with significant variation of the microstructure. Finally, the processing region with the occurrence of extensive DRX (around the condition of 1100 °C/0.01 s^{-1}) can be eventually recommended as the optimized processing window for the alloy, which also fits the prediction of the activation energy map (Fig.6).

3 Conclusions

1) The average activation energy of the alloy is calculated as 447.2 kJ/mol, and the constitutive equations and activation energy map are also established and constructed.

2) The hot processing map of the alloy is constructed at temperatures and strain rates of 700~1100 °C and 0.001~10 s^{-1}, respectively. Two peak domains are identified in the hot processing map, which are: 800~975 °C/0.001~0.01 s^{-1} and 1000~1100 °C/0.01~0.1 s^{-1}. The flow instability region locates under the conditions of strain rates higher than 1 s^{-1}.

3) The mechanism at the peak domains in the processing map is DRV or the combination of DRV and DRX. The presence of flow instability is attributed to external cracking, flow localization and local kinking.

4) The optimal processing window is recommended as high temperature (about 1100 °C) and medium-low strain rate (about 0.01 s^{-1}). The unstable deformation at flow instability region should be avoided in actual TMP.

References

1 Banerjee D, Williams J C. *Acta Materialia*[J], 2013, 61: 844

2 Zhu W G, Lei J, Tan C S *et al. Materials and Design*[J], 2019, 168: 107 640

3 Shi R P, Zheng Y F, Banerjee R *et al. Scripta Materialia*[J], 2019, 171: 62

4 Lin Y C, Huang J, He D G *et al. Journal of Alloys and Compounds*[J], 2019, 795: 471

5 Zhou W, Ge P, Zhao Y Q *et al. Rare Metal Materials and Engineering*[J], 2015, 44(10): 2415

6 Bao R Q, Huang X, Cao C X. *Transactions of Nonferrous Metals Society of China*[J], 2006, 16: 274

7 Hua K, Xue X Y, Kou H C *et al. Journal of Alloys and Compounds*[J], 2014, 615: 531

8 Fan J K, Kou H C, Lai M J *et al*. *Materials and Design*[J], 2013, 49: 945

9 Matsumoto H, Kitamura M, Li Y P *et al. Materials Science and Engineering A*[J], 2014, 611: 337

10 Zhou W, Ge P, Zhao Y Q *et al. Rare Metal Materials and Engineering*[J], 2012, 41(8): 1381

11 Zhou W. *Rare Metal Materials and Engineering*[J], 2016, 45(7): 1732

12 Li C, Zhang X Y, Li Z Y *et al. Materials Science and Engineering A*[J], 2013, 573: 75

13 Zhao Q Y, Yang F, Torrens R *et al. Materials Characterizations*[J], 2019, 149: 226

14 Sellars C M, McTegart W J. *Acta Metallurgica*[J], 1996, 14: 1136

15 Warchomicka F, Poletti C, Stockinger M *et al. Materials Science and Engineering A*[J], 2011, 528: 8277

16 Zhao Z, Xiao L, Ge P *et al. Materials Science and Engineering A*[J], 2014, 604: 111

17 Sun Y, Wan Z P, Hu L X *et al. Materials and Design*[J], 2015, 86: 922

18 Prasad Y V R K, Gegel H L, Doraivelu S M *et al. Metallurgical and Materials Transactions A*[J], 1984, 15: 1883

19 Murty S V S, Rao B, Kashyap B P. *International Materials Reviews*[J], 2000, 45: 15

20 Prasad Y V R K, Seshacharyulu T. *Materials Science and Engineering A*[J], 1998, 243: 82

铸态粗晶 Ti-5553 钛合金的高温变形行为与机理

赵秦阳[1]，陈永楠[1]，徐义库[1]，Leandro Bolzoni[2]，Fei Yang[2]

(1. 长安大学，陕西 西安 710064)

(2. 怀卡托大学，新西兰 汉密尔顿 3240)

摘　要：借助 Gleeble-3800 热模拟试验机研究了铸态粗晶 Ti-5553 合金在温度 700~1100 ℃、应变速率 0.001~10 s^{-1} 条件下的高温变形行为。结果表明，合金的流变应力对变形温度和应变速率都有强敏感性，流变软化过程也随变形参数的改变呈现出不同的模式。通过经典动力学模型，建立了合金高温变形的本构关系和激活能分布图，基于动态材料模型构建了合金的热加工图并实现了对不同加工区间变形机制的识别。合金在低温区（700 ℃）和高应变速率区（>1 s^{-1}）均展现出失稳变形的特征，包括外部开裂、绝热剪切带、局部流变等机制，在实际加工中应对这些加工区域进行规避。合金在 800 ℃及中低应变速率（<0.1 s^{-1}）变形下的主导机制为 α 相的动态析出，在中高温（900~1100 ℃）及中低应变速率变形下的主导机制为动态回复与动态再结晶的结合。此外，合金在高温较低应变速率（1100 ℃/0.01 s^{-1}）条件的变形中表现出大范围动态再结晶的行为特点并伴随稳定的流变软化，因此此条件附近的参数区间被认定为该合金的最优加工窗口，应在实际加工中给予优先考虑。

关键词：Ti-5553合金；高温变形行为；本构关系；加工图；变形机制

作者简介：赵秦阳，男，1993 年生，博士，长安大学材料科学与工程学院，陕西 西安 710064，电话：029-82337340，E-mail: zqy_ustb@163.com